Band Structure and Ballistic Electron Transport Simulations in GeSn Alloys

Suyog Gupta[#], Blanka Magyari-Köpe, Yoshio Nishi and Krishna C. Saraswat
Department of Electrical Engineering
Stanford University
Stanford, CA 94305 USA
[#] suyog@stanford.edu

***Abstract*—Electronic band structure of germanium-tin (GeSn) alloys is calculated using virtual crystal approximation (VCA) within the framework of the nonlocal empirical pseudopotential method (NL-EPM). Modifications to the conventional VCA are applied in order to account for structural and compositional disorder in the alloy. Using the results of band structure calculations, ballistic MOSFET simulations are carried out to gauge the performance benefits and design consideration of GeSn as a channel material for nMOSFETs**

***Index Terms*—GeSn, pseudopotential, bandstructure, nMOSFET**

I. Introduction

Substitution of Sn into Ge lattice to form semiconducting GeSn alloy has been found to result in a direct band gap material [1]. Tunable direct band gap and potential for high electron and hole mobilities [2] in GeSn has attracted significant research interest in realizing optoelectronic and high performance CMOS devices using GeSn. However large discrepancy exists in literature over the alloy Sn content at which the material exhibits direct band gap. Virtual crystal approximation (VCA) tight-binding calculations of [3] predict GeSn to become direct gap material for alloy Sn content > 20%. GeSn alloy band structure calculations using supercell mixed-atom method [4] find 17% Sn to induce an indirect to direct band gap transition. On the contrary, first principles electronic band structure calculations based on density functional theory (DFT) of Gupta et al [5] and Yin et al [6] predict much lower alloy Sn% of 8% and 6.3% respectively for the indirect to direct band gap transition in GeSn alloys. Although DFT based calculations have been shown to yield good agreement to experimentally observed GeSn band gaps, such a method necessitates calculations involving large supercells and incurs severe penalty in terms of computation time and complexity. Empirical methods that more accurately model the alloy properties are therefore desired.

In this work we employ the nonlocal empirical pseudopotential method (NL-EPM) to calculate band structure and effective masses in relaxed and strained GeSn alloys. VCA along with corrections for alloy disorder induced crystal potential fluctuations has been used to accurately model the electronic properties of GeSn. Subsequently, electron transport simulations have been performed in the ballistic regime in order to evaluate band structure effects on GeSn nMOSFET performance.

II. Nonlocal Empirical Pseudopotential

Following the work of Chelikowsky and Cohen [7], we write the single electron pseudo-Hamiltonian including the spin-orbit interaction as

$$H = -\frac{\hbar^2}{2m}\nabla^2 + V_{loc} + V_{nloc} + V_{so} \quad (1)$$

V_{loc}, V_{nloc} and V_{so} represent the local, nonlocal and spin orbit contributions to the pseudopotential respectively. A basis set consisting of 137 plane waves are used to expand the pseudopotential. For the alloy (both strained and unstrained) local component of pseudopotential at arbitrary reciprocal vector q is required and obtained by performing cubic spline interpolation between pseudopotential form factors V_s at q^2={0, 3, 8,11}* $(2\pi/a_0)^2$. As in [8] V_s at q^2=0 is extrapolated as $-2E_F/3$ where E_F is the free electron Fermi-energy. To ensure fast cut-off at large q^2 we have followed the approach of [9] and required

$$V_s(q) = V_{cubic}(q)\left(\tfrac{1}{2}\tanh\left(\frac{a_5 - q^2}{a_6}\right) + \tfrac{1}{2}\right), \quad (2)$$

$$V_{cubic}(q) = a_1 q^3 + a_2 q^2 + a_3 q + a_4$$

		Unit	Ge	Sn
Lattice constant		Å	5.646	6.490
Interpolation coefficients	a_1	atomic units	-0.1684	-0.1186
	a_2		0.4956	0.3159
	a_3		-0.0077	0.0809
	a_4		-0.5650	-0.4276
	a_5		5.0	4.0
	a_6		0.3	0.3

Table 1. Pseudopotential parameters used for Ge and Sn. Nonlocal and spin orbit parameters from [7]

The lattice constant of GeSn alloy has been taken as

ISBN 978-0-615-71756-2

$$a_{Ge_{1-x}Sn_x} = (1-x)a_{Ge} + xa_{Sn} - \theta_{GeSn}(1-x)x \qquad (3)$$

θ_{GeSn} is the lattice bowing parameter and assumed to be equal to -0.166Å [10].

III. Band Structure Calculations

Energy band gap E_g in semiconductor alloys exhibit a non linear dependence on alloy composition x and typically represented by a quadratic function in x as follows

$$E_g^{Ge_{1-x}Sn_x} = (1-x)E_g^{Ge} + xE_g^{Sn} - b_g(1-x)x \qquad (4)$$

b_g is called the band gap bowing parameter and measures the deviation of the alloy band gap from a linear interpolation between the band gaps of constituent elements. Experimental investigations of [11] have shown GeSn alloys to exhibit a large direct gap (Γ) bowing parameter b_g of ~2.1eV. EPM calculations using simple VCA, in which the alloy potential in the virtual crystal is modeled as composition weighted average of constituent element potentials, predicts a nearly linear dependence (b_g ~ 0eV) of GeSn alloy bandgap with increasing Sn mole fraction as shown in Fig. 1.

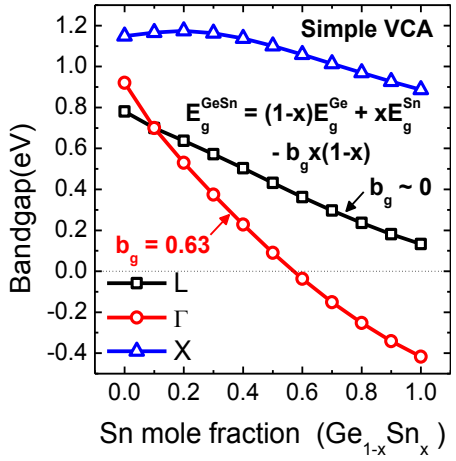

Fig. 1. Bandgap at critical points for GeSn alloys using simple VCA

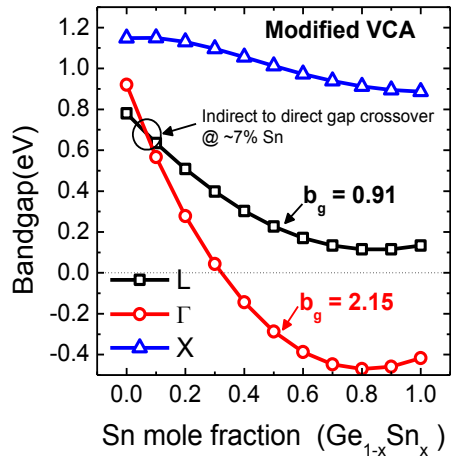

Fig. 2. Bandgap at critical points for GeSn alloys using VCA corrected for alloy compositional and structural disorder.

Using DFT based electronic structure calculations; Yin et al [6] have attributed the band gap bowing b_g underestimation to the lack of adequate description of structural disorder in systems with large lattice mismatch such as Ge and Sn by the potential-averaged VCA formalism. To correctly account for the large band gap bowing in GeSn, we have introduced a correction term to VCA alloy potentials to represent the combined effect of structural and compositional disorder, similar to the approach described in [12]. Within the framework of the NL-EPM, disorder correction is applied only to the local component of alloy pseudopotential and given by

$$V_{loc}^{Ge_{1-x}Sn_x}(q) = (1-x)\frac{\Omega_{Ge}}{\Omega_{Ge_{1-x}Sn_x}}V_{loc}^{Ge}(q) + x\frac{\Omega_{Sn}}{\Omega_{Ge_{1-x}Sn_x}}V_{loc}^{Sn}(q) - (1-x)xP_{loc}\frac{\left(\Omega_{Ge}V_{loc}^{Ge}(q) - \Omega_{Sn}V_{loc}^{Sn}(q)\right)}{\Omega_{Ge_{1-x}Sn_x}} \qquad (5)$$

Ω is the unit cell volume, x is the mole fraction of Sn in the alloy and P_{loc} is treated as a fitting parameter to achieve direct gap bowing parameter b_g in agreement with experimental data of [11] as shown in Fig. 2. The indirect to direct band gap transition has been found to occur at alloy Sn% of 7%. Also, negligible change in Δ energy gap has been observed for Sn composition < 20%, causing an increase in L-Δ gap.

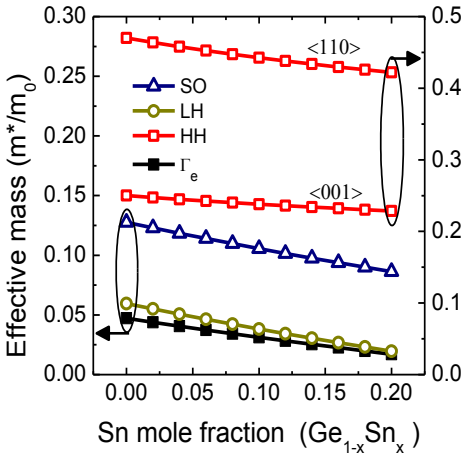

Fig. 3. Calculated electron and hole effective masses at Γ point as a function of Sn composition in GeSn.

The curvature effective masses calculated at Γ point shown in Fig. 3, decreases for both electrons and holes as Sn content is increased in GeSn. We also find electron effective masses in GeSn at L and Δ minimum to be practically unchanged from those in Ge.

IV. Ballistic Electron Transport Simulations

Using the results from EPM band structure calculations and employing Natori's ballistic MOSFET model [13] we the estimate inversion charge densities, sub-band structure and

source injection velocity (V_{inj}) in a double gate nMOSFET structure with 20nm body thickness and 0.5nm EOT with Ge or GeSn as channel material. The substrate is assumed to be (001) oriented and the channel direction considered is along <110>. Fig. 4 shows the projection of equivalent conduction band valleys in Ge, GeSn on the k_x-k_y plane. $L_{||}$ indicates L valleys with major axis along the channel direction and have larger transport effective mass than the $L_{\perp}$ valleys. In-plane Δ valleys (Δ_4) and out-of-plane Δ valleys (Δ_2) have degeneracy of 4 and 2 respectively.

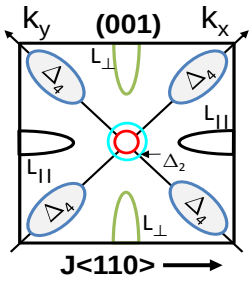

Fig. 4. Projection of equivalent conduction band valleys on the k_x-k_y plane for (001) oriented substrate.

Fig. 5 shows the calculated relative valley occupancies as a function of applied gate bias for Ge and unstrained GeSn (10%Sn) as channel material. Since $L_{||}$ and $L_{\perp}$ valleys have same effective mass (m_z) in the confinement direction (out-of-plane), they are equally populated. In case of Ge, a large energy separation of 140meV between Γ and L valleys prevents any significant population of Γ valley. At high gate bias, large sub-band splitting in L valleys causes carrier spill

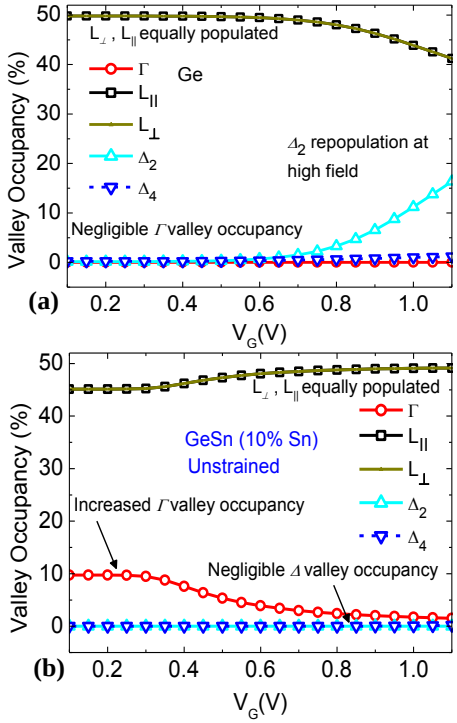

Fig. 5. Relative valley occupancy for (a) Ge and (b) Unstrained GeSn (10% Sn) channel double gate nMOSFETs.

over to Δ_2 valley with larger confinement effective mass (m_z) and high transport effective mass ($m_{||}$). From NL-EPM calculations of Fig. 2, we find unstrained GeSn with 10% Sn to be direct bandgap with Γ valley ~40meV below L valley. As a result, increased population of low $m_{||}$ Γ valley is observed in GeSn with 10% Sn. Alloying with Sn lowers both Γ and L valleys without significantly affecting the Δ valley thereby eliminating the carrier spill over to Δ valley observed in Ge.

Population of valleys with low effective mass in the transport direction results in increase in the source injection velocity V_{inj} and the ballistic drive current of the device. As shown in Fig. 6, for direct gap GeSn (Sn > 7%) increased population of Γ valley boosts V_{inj}. For both direct gap (10% Sn) and indirect gap (6% Sn) GeSn, increase in L-Δ energy gap inhibits Δ valley occupancy at large gate voltages and prevents the V_{inj} degradation seen in Ge. Thus, improvement over Ge nMOSFETs in terms of electron V_{inj} (or equivalently, ballistic drive current) can be expected for GeSn channel nMOSFETs throughout the operating gate voltage range.

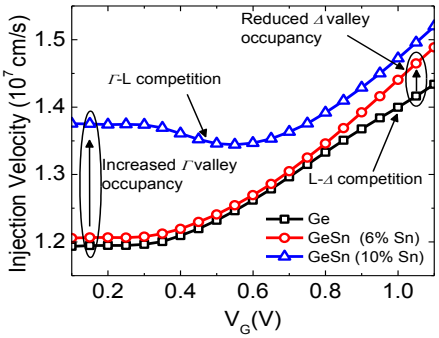

Fig. 6. Comparison of source injection velocity (V_{inj}) double gate nMOSFETs with Ge, unstrained GeSn (6%Sn, 10%Sn) channel.

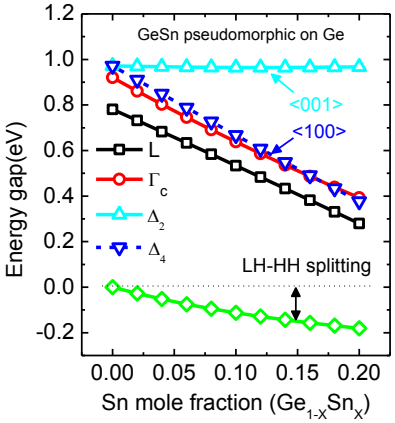

Fig. 7. Band gap at critical points for GeSn grown on Ge. GeSn layer is under biaxial compression when grown epitaxially on Ge (001).

We also analyze the implications of GeSn growth using Ge buffer on nMOSFET performance. Current state of the art GeSn growth relies on a Ge buffer to achieve defect free epitaxial growth [14]. Due to the larger lattice constant of GeSn than Ge, GeSn is fully biaxially compressed

(pseudomorphic) with respect to Ge when grown epitaxially on Ge. From EPM calculations we find biaxial compression to increase the direct gap and reduce L-Δ_4 energy gap as shown in Fig. 7. Interestingly, unlike in case of unstrained GeSn no indirect to direct band gap transition is observed for GeSn grown pseudomorphic to Ge. As shown in Fig. 8**,** for compressively strained GeSn negligible Γ valley occupancy is observed and electrons preferentially fill high effective mass Δ_4 valleys causing a reduction in V_{inj}. Hence, compression in GeSn layer resulting from growth on Ge offsets any improvements in nMOSFET performance expected from GeSn.

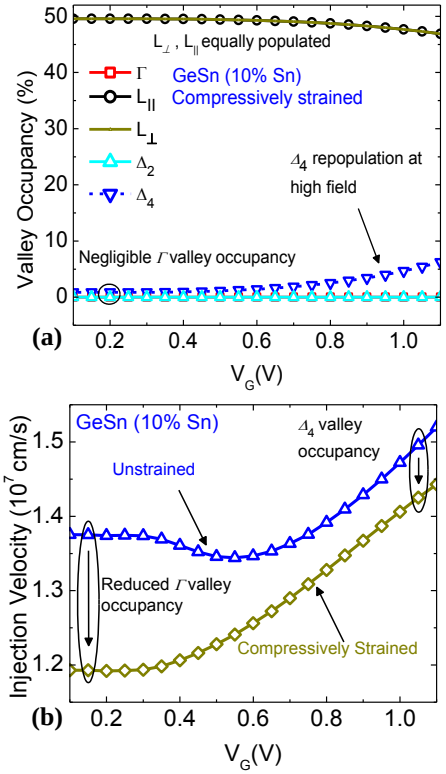

Fig. 8. (a) Relative valley occupancy for GeSn compressively strained with respect to Ge. (b) Comparison of V_{inj} for strained and unstrained GeSn (10%Sn) channel double gate nMOSFETs.

V. Conclusions

In this work we present an empirical pseudopotential based method to calculate electronic band structure of GeSn alloys. Applying corrections to the virtual crystal potential in order to account for the large lattice mismatch between Ge and Sn has been shown to reproduce band gaps in agreement with experiments. Analysis based on ballistic transport model has been used to provide valuable insights into material requirements for CMOS using GeSn channel. We find that significant benefits in nMOSFET performance can be achieved by employing GeSn as channel. However, compressive strain in GeSn grown on Ge has been shown to offset any gain in nMOSFET performance obtained by alloying Ge with Sn. Enhancement in GeSn nMOSFETs can be obtained by growth of GeSn on relaxed SiGeSn buffer layers in order to achieve strain-free GeSn or introduce tensile strain in GeSn channel.

Acknowledgement

This work has been supported by the Focus Center for Materials, Structures and Devices (MSD). S. Gupta would like to acknowledge financial support from the Stanford Graduate Fellowship.

References

[1] G. He and H. A. Atwater, "Interband transitions in Sn_xGe_{1-x} alloys", *Phys. Rev. Lett.*, vol. 79, pp. 1937, 1997

[2] J. D. Sau and M. L. Cohen, "Possibility of increased mobility in Ge-Sn alloy system", *Phys. Rev. B*, vol. 75, pp. 5208, 2007.

[3] D. W. Jenkins and J. D. Dow, "Electronic properties of metastable Ge_xSn_{1-x} alloys", *Phys. Rev. B*, vol. 36, no. 15, pp. 7994, 1987.

[4] P. Moontragoon, Z. Ikonić and P. Harrison, "Band structure calculations of Si-Ge-Sn alloys: achieving direct band gap materials", *Semicond. Sci. Technol.*, vol. 22, pp. 742, 2007.

[5] S. Gupta et al., "GeSn Technology: Extending Ge Electronics Roadmap" in *IEDM Tech. Digest.*, 2011, pp. 398.

[6] W.-J. Yin, X.-G. Gong and S.-H. Wei, "Origin of unusually large band-gap bowing and the breakdown of the band-edge distribution rule in Sn_xGe_{1-x} alloys", *Phys. Rev. B*, vol. 78, pp. 161203, 2008.

[7] J. R. Chelikowsky and M. L. Cohen, "Nonlocal pseudopotential calculations for the electronic structure of eleven diamond and zinc-blende semiconductors", *Phys. Rev. B*, vol. 14, pp. 556, 1976.

[8] M. M. Rieger and P. Vogl, "Electronic-band parameters in strained $Si_{1-x}Ge_x$ alloys on $Si_{1-x}Ge_x$ substrates", *Phys. Rev. B*, vol. 48, pp. 14276, 1993.

[9] P. Friedel, M. S. Hybertsen and M. Schlüter, "Local empirical pseudopotential approach to the optical properties of Si/Ge superlattices", *Phys. Rev. B*, vol. 39, pp. 7974, 1989.

[10] J. Kouvetakis, J. Menendez and A.V.G Chizmeshya, "Tin-based group IV semiconductors", *Annu. Rev. Mat. Res.*, vol. 36, pp. 497-554, 2006.

[11] R. Chen, H. Lin, Y. Huo, C. Hitzman, T. I. Kamins and J. S. Harris, "Increased photoluminescence of strain-reduced, high Sn composition $Ge_{1-x}Sn_x$ alloys grown by molecular beam epitaxy", *Appl. Phys. Lett.*, vol. 99, pp. 181125, 2011.

[12] S. J. Lee, T. S. Kwon, K. Nahm and C. K. Kim, "Band structure of ternary compound semiconductors beyond the virtual crystal approximation", *J. Phys. Condens. Matter*, vol. 2, pp. 3253, 1990.

[13] K. Natori, "Ballistic metal-oxide-semiconductor field effect transistor", *J. App. Phys.*, vol. 76, pp. 4879, 1994.

[14] B. Vincent et al., "Undoped and *in-situ* B doped GeSn epitaxial growth on Ge by atmospheric pressure-chemical vapor deposition", *Appl. Phys. Lett.*, vol. 99, pp. 152103, 2011.